Desalination and Water Treatment
www.deswater.com
doi: 10.5004/dwt.2021.26567

210 (2021) 377–392
January

Amino functionalized zirconia as novel adsorbent for removal of Cr(VI) from aqueous solutions: kinetics, equilibrium, and thermodynamics studies

Tahira Mahmood*, Abid Ullah, Rahmat Ali, Abdul Naeem, Muhammad Farooq, Madeeha Aslam

National Center of Excellence in Physical Chemistry, University of Peshawar, Peshawar 25120, Pakistan, Tel. +92 3329266988; email: tahiramahmood@uop.edu.pk (T. Mahmood)

Received 17 January 2020; Accepted 9 September 2020

ABSTRACT

An effective hybrid adsorbent based on zirconia (ZrO_2) and 3-aminopropyltriethoxysilane (APTES) was prepared for the removal of Cr(VI) from aqueous solutions. Co-precipitation method was used to prepare nano-crystalline zirconia (ZrO_2) while its functionalization with 3-aminopropyltriehoxysilane (APTES) was carried out by grafting method. The characterization of ZrO_2 and functionalized zirconia (NH_2–ZrO_2) was performed by Fourier transform infrared (FTIR) spectroscopy, X-ray diffraction analysis, scanning electron microscopy (SEM), and thermogravimetric analysis. The presence of carbon (10.73%), nitrogen (2.07%), silicon (0.15%), and a rise in the percentage of oxygen (from 26.79% to 28.23%) in the energy dispersive X-ray spectra of NH_2–ZrO_2 supported by FTIR analysis, showed that ZrO_2 has been successfully functionalized with APTES. The adsorption characteristics of NH_2–ZrO_2 for the removal of Cr(VI) were examined by the batch method. Adsorption was found to be highly dependent on solution pH, contact time, Cr(VI) initial concentration, and adsorbent dosage. Kinetic data was explained well by pseudo-second-order kinetic model, while the equilibrium data were best fitted the Langmuir model with a maximum adsorption capacity of 17.89 mg/g at 298 K. The thermodynamic parameters, that is, negative values of $\Delta H°$ and $\Delta G°$ confirmed the exothermic and spontaneous nature of adsorption process.

Keywords: Co-precipitation method; Amino functionalized zirconia; Adsorption; Cr(VI); Kinetic models; Thermodynamic parameters

1. Introduction

Chromium has gained the attention of the scientific community because of its adverse effects on the surrounding environment and public health. The stable oxidation states of Cr are Cr(III) and Cr(VI), which exhibit different toxicities. Cr(III) is considered as an important micronutrient, while Cr(VI) is among the 16 most teratogenic and carcinogenic toxic pollutants in the world [1,2]. The major sources that discharge Cr(VI) into the water streams include effluents from various industries like leather tanning, electroplating, metal finishing, wood protection, electrical, and electronic equipment manufactures, chromium mining pigments, and catalysis [3]. According to World Health Organization (WHO), the highest permitted value of Cr(VI) in drinking and wastewater is 0.05 and 0.2 μg/mL, respectively [4]. Exceeding concentration of Cr(VI) from their permitted level can cause different health hazards like ulceration, liver damage, epigastric pain, hemorrhage, severe diarrhea, bronchitis, bronchogenic carcinoma, nausea, pulmonary congestion, vomiting, and cancer in the digestive tract and lungs [2]. Hexavalent species of chromium mainly exist as chromate ion (CrO_4^{2-}), hydrogen chromate ion ($HCrO_4^-$), chromic acid (H_2CrO_4), and its salts which depend on solution pH. The predominant species of Cr(VI) are H_2CrO_4

* Corresponding author.

predominant at solution pH less than 1, $HCrO_4^-$ predominant at pH values between 1 and 6, and CrO_4^{2-} predominant when solution pH is above 6.

Different methods like ion exchange, chemical precipitation, advanced oxidation techniques, filtration, electrodeposition, and adsorption have been applied for the purification of contaminated water [5]. Majority of these methods are not satisfactory due to the high cost, less efficiency, large amount of sludge formation, and inapplicability [6]. Adsorption is the most useful method for wastewater treatment because of its low cost, simple operation, applicability at very low concentrations, little sludge generation, suitability for using batch and continuous processes, and reusability of the adsorbents [7]. However, the most important factor in adsorption is the selection of efficient and novel adsorbent.

Different types of adsorbents have been tested such as activated carbon [8,9], zeolites [10], clays [11], and agricultural waste [12] to remove heavy metal ions from polluted water. The major issues with these adsorbents are their slow adsorption kinetics, low adsorption power, difficulties in regeneration and separation, and their comparatively weak interactions with heavy metals ions. Recently, various types of nanomaterials, for example, nanostructure zirconia [13], nanostructure alumina [14], and nanostructure titania [15] have been used for the detoxification of contaminated water. Nanomaterials have grabbed the attention of the scientific community due to their unique properties, such as faster adsorption kinetics, high adsorption capacity, simple operation, and quick responses [16]. The direct use of nanomaterials in adsorption study is not favorable because of their non-selectivity, less stability, and agglomeration in liquid phase [17]. To overcome these problems, the surface of nanomaterials can be functionalized with certain groups which make it selective and prevent agglomeration [18].

Nanocrystalline zirconia (ZrO_2) can be used as a support because of its attractive properties such as non-toxicity, very low solubility in water, good resistance to acids, bases, and oxidizing agents and high thermal stability [13]. The surface of ZrO_2 is amphoteric in nature due to the presence of Bronsted basic and acidic groups and Lewis acid–base Zr^{4+}–O^{2-} pairs. The ZrO_2 polymorphs surface have –OH groups which are important in surface structure and surface chemistry [19]. The surface functionalization of ZrO_2 has already been reported by many researchers. Zhou et al. [20] reported the functionalization of ZrO_2 surface by vinyl groups. Tarafdar and Pramanik [21] reported the functionalization of ZrO_2–SiO_2 mixed oxide by amino groups however there are few reports on the functionalization of ZrO_2 by amino groups. Luo et al. [22] reported the functionalization of ZrO_2 by amine groups using post-synthesis method. Silanes are silicon containing monomeric compounds in which silicon atom is attached to four substituent groups. Silanes have been frequently used for the functionalization of metal oxide surfaces. The basic advantages of using silanes in surface chemistry are that they can have different functional groups, for example, amino, carboxylic acid, cyano, etc., which can be easily introduced to metal oxide surface in one step [23,24]. Amino functionalizations have gained importance recently because of their high potential applications. Functionalization of mesoporous silica with amine groups has been reported by Ostwal et al. [25], Stoltenberg and Seidel-Morgenstern [26], and Sakamoto et al. [27].

In the present study, the surface of ZrO_2 particles is functionalized by amino groups of aminopropyltriethoxy silane (APTES). The prepared amino functionalized zirconia (NH_2–ZrO_2) particles were used for the adsorption of Cr(VI) from aqueous solutions. Reported literature survey shows that adsorption of Cr(VI) has not been explored yet using amino functionalized zirconia (NH_2–ZrO_2) as novel green adsorbent. This study emphasizes the effect of different sorption parameters on Cr(VI) adsorption and focuses on the investigation of the mass transfer limitations, kinetic, and thermodynamics features so as to develop a probable mechanism for Cr(VI) adsorption by NH_2–ZrO_2.

2. Experimental setup

2.1. Reagents and chemicals

Zirconium oxychloride octahydrate ($ZrOCl_2{\cdot}8H_2O$, 99%), 3-aminopropyltriethoxysilane ($C_9H_{23}NO_3Si$, 98%), and potassium dichromate ($K_2Cr_2O_7$) were provided by Merck while 1,5 diphenyl carbazide ($C_{13}H_{14}N_4O$, 98%) and acetone (C_3H_6O, 99%) were provided by Scharlau. Sulfuric acid (H_2SO_4, 98%) and sodium hydroxide (NaOH, 97%) were provided by BDH suppliers. Hydrochloric acid (HCl, 37%) was supplied by Riedel-de-Haen. Deionized water was used throughout the research work.

2.2. Adsorbent preparation

2.2.1. Synthesis of nanocrystalline zirconia

Nanocrystalline zirconia (ZrO_2) was prepared by co-precipitation method. First 450 mL of 0.088 M NaOH solution was taken in 1,000 mL round bottom flask. Then 4 g of solid $ZrOCl_2{\cdot}8H_2O$ was added with stirring which yielded a white turbid solution. The solution was stirred for 4 h and then filtered through Whatman no 42 filter paper. The gel obtained was washed with 0.5 L of deionized water to leach out the chloride ions. The chloride ions in filtrate were tested by silver nitrate solution. The washed gel was calcined at 823 K for 5 h in Nabertherm P330MB2 Furnace. The obtained powder was further characterized by different spectroscopic techniques.

2.2.2. Functionalization of nanocrystalline zirconia

The surface of nano-crystalline ZrO_2 was functionalized by treatment with 3-aminopropyltriethoxysilane (APTES). Nano-crystalline ZrO_2 (100 mg) was added to 10 mL acetone and 1 mL of APTES was dissolved in 9 mL H_2O. The mixture was then sonicated for 2 h using a Sonicator (POWERSONIC-405). The reaction mixture was centrifuged in tabletop centrifuge DSC200-2. Afterward, it was washed with deionized water two times to remove the unattached coupling agent molecules followed by drying for 4 h to obtain the amino functionalized nano-crystalline zirconia (NH_2–ZrO_2). The overall process for synthesis and functionalization of nanocrystalline zirconia is schematically presented in Fig. 1.

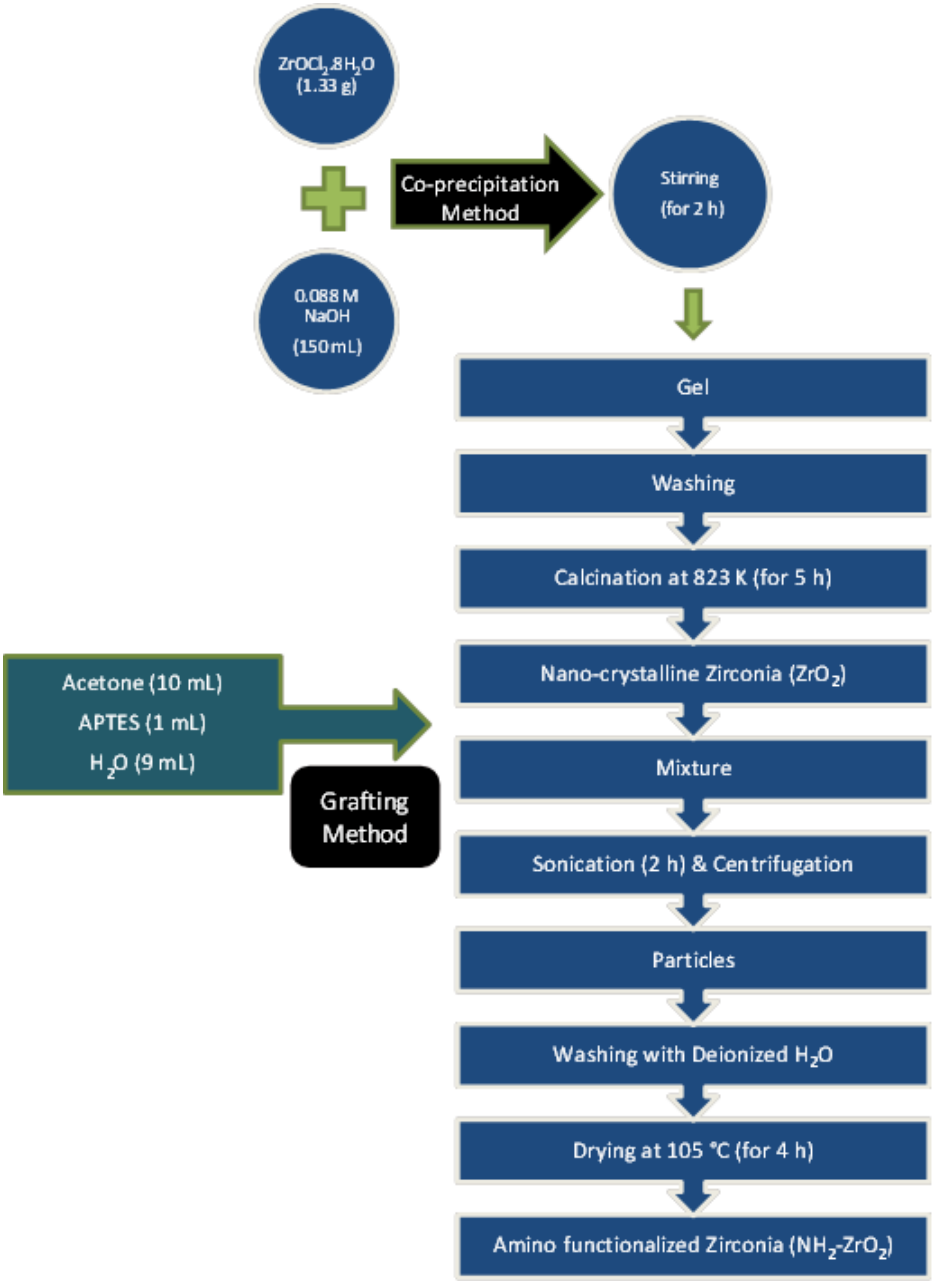

Fig. 1. Schematic diagram for preparation of amino functionalized zirconia (NH_2–ZrO_2).

2.3. Adsorbent characterization

Nano-crystalline ZrO_2 and functionalized NH_2–ZrO_2 were characterized using different analytical techniques. XRD analysis was carried out to get deeper knowledge about the crystallography and the crystallite size of ZrO_2 and NH_2–ZrO using JEOL X-ray diffractometer (model JDX-3532) with manganese filtered copper-kα radiations. The X-ray patterns were obtained by determining 2 theta (2θ) values ranging from 10° to 70° with step size of 0.04° and a step time of 0.5 s. The applying current and voltage were fixed at 30 mA and 40 kV respectively. The microstructures were examined by using scanning electron microscopy (SEM; JSM-6490, JEOL, Japan) at 20 keV. Elemental analysis of ZrO_2 and NH_2–ZrO_2 were performed by energy dispersive X-ray (EDX) micro analyzer spectrophotometer (EDX Inca-200, UK). Thermal analyses (TGA/DTA) were carried out in the temperature range 40°C–800°C at a heating rate of 10°C/min in the presence of continuous N_2 flow, using Perkin-Elmer Pyris1 analyzer. Surface chemistry and chemical structure of ZrO_2 and NH_2–ZrO_2 was studied using a Fourier transform infrared (FTIR) spectrophotometer (FTIR-2000, Perkin Elmer). Point of zero charge (pH_{PZC}) was determined by salt addition method [28] using 0.1 M $NaNO_3$ solution as electrolyte. In a typical procedure 40 mL of 0.1 M $NaNO_3$ solution was taken in a series of 100 mL polyethene

bottles with pH adjusted from 2 to 11. Then 100 mg of NH_2–ZrO_2 was added to each bottle and were kept in a shaking bath SHELAB (model WS17-2) at shaking rate of 140 rpm at 298 K. After 24 h the bottles were taken out and its final pH was recorded. The change in pH ($pH_f - pH_i$) was plotted against initial pH_i.

2.4. Adsorption procedure and regeneration of adsorbent

To study the effect of various parameters such as solutions pH, equilibrium time, media dosage, temperature, and adsorbates concentration on adsorption of Cr(VI) by NH_2–ZrO_2, batch experiments were performed. A known amount of NH_2–ZrO_2 was added to 40 mL of Cr(VI) solution taken in series of 100 mL bottles which were then placed in shaker bath at constant temperature and agitated at 120 rpm for definite time. After equilibration the solution was filtered to remove adsorbent particles and analyzed for the residual concentration of Cr(VI) at the wavelength of maximum absorbance (λ_{max}) using spectroscopic technique. The adsorption loading per unit mass of NH_2–ZrO_2, q_e (mg/g), and percentage adsorption were calculated by using the following equation:

$$q_e = \left(\frac{C_i - C_e}{1{,}000 \times m}\right) V \tag{1}$$

$$\text{Removal efficiency} = \left(\frac{C_i - C_e}{C_i}\right) \times 100 \tag{2}$$

where q_e (mg/g) is the amount of adsorbate adsorbed, C_i (mg/L) is the initial concentration of solution, C_e (mg/L) is the equilibrium concentration, V (L) is the volume of solution, while m (g) is the mass of adsorbent added.

The regeneration study was carried out by adding 1 g NH_2–ZrO_2 into 200 mL of 58.35 mg/L Cr(VI) solution. The pH of mixture was adjusted to 2 and stirred at 300 rpm for 30 min at 298 K. The Cr(VI) loaded adsorbent was collected by filtration, rinsed, and dried. The used adsorbent was immersed in 200 mL NaOH solution (0.1 N) and stirred under the same condition as those used in adsorption study. At the end of desorption experiments, the surface collected was washed, dried, and recycled. Six consecutive adsorption–desorption cycles were executed.

2.4.1. Cr(VI) analysis

There are many methods available for Cr(VI) determination, such as atomic absorption spectrometry (AAS), ion chromatography (IC), inductively coupled plasma-mass spectrometry (ICP-MS), inductively plasma-optical emission spectrometry (ICP-OES), etc., but they are expensive and require technical skills. The inexpensive, quick, and easy way for Cr(VI) determination in solution is diphenyl carbazide spectrophotometric method [1]. Absorbance values were determined at the corresponding λ_{max} (540 nm) by preparing a colored complex of Cr(VI) with 1,5-diphenylcarbazide in the presences of sulfuric acid by using UV-spectrophotometer (UV-160A, Shimadzu, Japan). The absorbance was then changed into concentration data by utilizing the calibration relation.

2.4.2. Kinetics study

Kinetics of adsorption process was studied to observe the effect of contact time and determine kinetic parameters. A specific amount of NH_2–ZrO_2 (0.1 g) was added to 40 mL of Cr(VI) solutions (197 mg/L) in series of 100 mL bottles and agitated in thermostatic shaker at 120 rpm at constant temperature (298, 303, and 308 K). The bottles were taken out of shaker bath after specific time intervals, filtered to remove adsorbent particles and analyzed for Cr(VI) concentration in filtrate.

The kinetics and mechanism of Cr(VI) adsorption was analyzed using different kinetics models such as using pseudo-first-order, pseudo-second-order, Elovich, intraparticle diffusion, and Boyd models. In 1889 Lagergren introduced a first-order kinetic model to interpret the kinetics of liquid–solid phase adsorption. The linear for of this model is given as follows:

$$\log\left(q_e - q_t\right) = \log q_e - \left(\frac{k_1}{2.303}\right) t \tag{3}$$

where k_1 (min^{-1}) represents the rate constant, q_e (mg/g) shows the adsorption capacity, q_t (mg/g) refers to the uptake at any time (t).

In 1995, Ho introduced second-order equation for the adsorption of species from solution as can be expressed as:

$$\frac{t}{q_t} = \frac{1}{V_0} + \frac{1}{q_e} t \tag{4}$$

$$V_0 = k_2 q_e^2 \tag{5}$$

In 1934 Zeldowitch, presented a kinetic equation for chemisorption reactions called Elovich equation. Basically, this equation was developed for the kinetics of gases adsorb on heterogeneous solid surfaces. Recently this equation has been applied for the adsorption of metal ions from solutions. The general form of this equation is expressed [29] as:

$$\frac{dq_t}{dt} = \alpha e_t^{-\beta q} \tag{6}$$

To simplify the above equation, apply boundary conditions, that is, "$q_t = 0$ at $t = 0$ and $q = q_t$ at $t = t$ while taking $\alpha\beta >> t$."

$$q_t = \frac{1}{\beta}\ln\left(\alpha\beta\right) + \frac{1}{\beta}\ln t \tag{7}$$

where q_t (mg/g) is the amount of adsorbate adsorbed at specific time, α is the initial rate of adsorption while β is the desorption constant.

Intraparticle diffusion model was presented by Weber and Morris [30]. According to this model, the uptake of solute particles from a solution is directly proportional

to $t^{1/2}$ rather than contact time. Mathematically this model can be represented [31] as:

$$q_t = R_{id}\, t^{1/2} + C_i \tag{8}$$

where R_{id} (mg/g/min$^{1/2}$) is the intraparticle diffusion rate constant while C_i is the boundary layer thickness. If the plot of "q_t vs. $t^{1/2}$" give a straight line and passing from the origin with slope R_{id}, and intercept C_i, mean that the data follows Weber and Morris.

The kinetic data were further analyzed by Boyd model for the determination of real rate-limiting step (intra-particle diffusion or film diffusion). Boyd equation can be represented [32] as:

$$F = 1 - \left(\frac{6}{\pi^2}\right)\sum_{m}^{1}\left(\frac{1}{m^2}\right)\exp\left(-m^2 B_t\right) \tag{9}$$

$$F = \frac{q_t}{q_e} \tag{10}$$

Rearranging the above equation:

$$B_t = -0.4977 - \ln\left(1 - F\right) \qquad \text{when } F > 0.85 \tag{11}$$

$$B_t = \left[\sqrt{\pi} - \sqrt{\pi - \left(\pi^2 F / 3\right)}\right]^2 \qquad \text{when } F < 0.85 \tag{12}$$

Here F is the fractional attainment and B_t represents a function of F while m is the integer which defines the solution infinite series. Moreover, q_e and q_t are maximum sorption capacities at equilibrium and time t, respectively.

2.4.3. Equilibrium isotherm study

Equilibrium isotherm studies were carried out by adding a specific amount of NH_2–ZrO_2 (0.1 g) to different initial concentration (9.90–283.20 mg/L) of Cr(VI) solutions with their pH adjusted at 2. The resulting mixtures were oscillated at 120 rpm in shaking bath at constant temperature (298, 308, and 318 K). The samples were filtered and analyzed by UV-spectrophotometer. The experimental data were analyzed using different adsorption isotherm models.

In 1909, Freundlich presented an empirical model for the adsorption on heterogeneous surfaces. The general form of Freundlich adsorption isotherm is presented as [33].

$$q = K_f C_e^{1/n} \tag{13}$$

The linear form of this isotherm is represented by the following equation:

$$\log q = \log K_f + \frac{1}{n}\log C_e \tag{14}$$

where C_e (mg/L) is equilibrium concentration, q (mg/g) is mount of adsorbate adsorbed, K_f is Freundlich constant, and n is the adsorption intensity.

In 1916, Langmuir presented a semi-empirical model for the adsorption of adsorbates on homogeneous surface of adsorbent. The basic consideration of this model is the fixed number of adsorptive sites on adsorbent surface, which leads to the monolayer adsorption. The more conventional form of Langmuir isotherm is represented [34] as:

$$\frac{C_e}{q_e} = \frac{1}{K_b q_m} + \frac{C_e}{q_m} \tag{15}$$

where q_e (mg/g) is the adsorption capacity, q_m (mg/g) is the maximum monolayer adsorption capacity, while K_b (L/mg) is binding energy constant.

The Temkin adsorption model assumed that the decrease in adsorption energy is linear instead of logarithmic, as expressed in the Freundlich equation. The decrease in adsorption energy with an increase of surface coverage is due to the solute-solid interaction. The general form of Temkin isotherm is expressed [35] as:

$$q_e = \frac{RT}{b}\ln A_T C_e \tag{16}$$

While the linear form of this isotherm is written as:

$$q_e = B_T \ln A_T + B_T \ln C_e \tag{17}$$

$$B_T = \frac{RT}{b} \tag{18}$$

where T (K) is the absolute temperature, R (8.314 J/mol k) is Universal gas constant, A_T (L/mg) is Temkin isotherm constant while b is Temkin constant related to adsorption energy.

Dubinin–Radushkevich (D–R) model [36] is an empirical isotherm used for the adsorption process that take place on both heterogeneous and homogeneous surfaces. This model predicts the type of adsorption process from adsorption energy. The linear form of D–R adsorption isotherm is expressed as:

$$\ln q_e = \ln q_{D-R} - \beta\varepsilon^2 \tag{19}$$

where ε is Polanyi potential given with $\varepsilon = RT\ln(1 + 1/C_e)$ and constant q_{D-R} (mg/g) correspond to maximum monolayer uptake capacity. While β (mol^2/J^2) is a constant associated to the adsorption energy E (kJ/mol) by the equation as given below:

$$E = \frac{1}{\sqrt{2\beta}} \tag{20}$$

3. Results and discussion

3.1. Characterization

3.1.1. X-ray diffractometry (XRD)

XRD is very useful technique used for the identification of unknown solid samples. It gives information about phase

transformation, crystallinity, and unit cells dimensions of the sample. The XRD pattern of ZrO_2 and NH_2–ZrO_2 is presented in Fig. 2. It can be seen that ZrO_2 is highly crystalline in nature. The peaks appeared at *d* spacing values of 5.075, 3.66, 3.157, 2.84, 2.674, 2.535, 2.498, and 1.659 with respective miller indices (001), (110), (–111), (111), (002), (–201), and (221) corresponding to monoclinic ZrO_2 (JCPDS card No: 37–1484). Furthermore, the peaks observed at d spacing values of 2.947, 2.181, 1.811, and 1.510 with corresponding miller indices (111), (112), (220), and (311) correspond to tetragonal ZrO_2 (JCPDS card No: 17–923). The XRD pattern is dominated by the characteristic peaks of the monoclinic structure, suggesting that the sample is mainly in the monoclinic phase. Similar observations have been reported by Sadiq et al. [37] and Guerrino et al. [38]. Crystallite size of ZrO_2 particles were calculated using Debye Scherer's equation given below:

$$\text{Crystallite size} = \frac{0.9\lambda}{B\cos\theta} \tag{21}$$

where λ is the wavelength of X-ray, B is the line broadening full width at half maximum (FWHM) of Bragg peak, and θ is the angle of reflection. The crystallite size calculated for monoclinic phase with the help of Scherer's equation is 13.89 nm, which is comparable in magnitude with the values reported for monoclinic ZrO_2 by Stoe et al. [39]. The same set of XRD peaks were observed for NH_2–ZrO_2 showing the crystalline phase stability of ZrO_2 during surface functionalization.

3.1.2. Surface morphology and EDX analysis

The microstructures and EDX spectra of ZrO_2, NH_2–ZrO_2, and Cr(VI) loaded NH_2–ZrO_2 are given in Figs. 3a–f. The SEM micrograph of ZrO_2 shows spherical particles morphology which is highly agglomerated. The surface morphology of NH_2–ZrO_2 (Fig. 3c) is totally different from ZrO_2 which may be due to the attachment of coupling agent on the surface. As can be seen (Fig. 3e) the SEM images of Cr(VI) loaded NH_2–ZrO_2 shows higher agglomeration of particles after adsorption. The percentage of different elements observed in EDX spectra of ZrO_2 and NH_2–ZrO_2 is presented in Figs. 3b and d, respectively. The spectra of ZrO_2 (Fig. 3b) show the peaks only for zirconium and oxygen, indicating that the prepared ZrO_2 is free from impurities. The chemical composition data obtained from EDX analysis are tabulated in the EDX table (Fig. 3b), which shows the weight percentage of zirconium and oxygen is 73.21% and 26.79%, respectively. Similar results were obtained by Sadiq et al. [37] while using ZrO_2 as a catalyst for the oxidation of isopropanol to acetone. The EDX spectra of NH_2–ZrO_2 (Fig. 3d), shows some additional peaks for carbon (10.73%), nitrogen (2.07%), and silicon (0.15%) which confirms the successful attachment of silane coupling agents on ZrO_2 surface. Whereas the EDX analysis of Cr(VI) loaded NH_2–ZrO_2 (Fig. 3f) shows additional peaks for Cr(VI) which confirms the adsorption of Cr(VI) onto NH_2–ZrO_2.

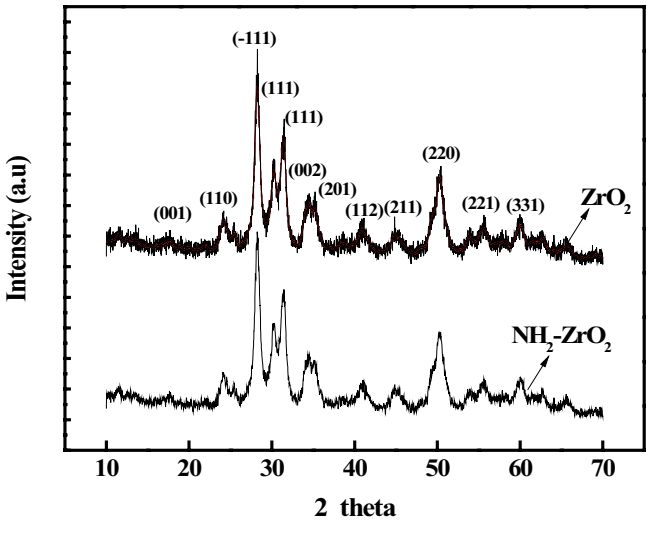

Fig. 2. XRD pattern of ZrO_2 and NH_2–ZrO_2.

3.1.3. FTIR analysis

FTIR spectroscopy was employed to get information about the surface functional groups and chemical structure. The FTIR spectra of ZrO_2 and NH_2–ZrO_2 were recorded in the range of 4,000–450 cm^{-1} as shown in Fig. 4. The spectra of ZrO_2 showed five characteristic peaks. The absorption peaks in the range of 490–745 cm^{-1} corresponds to the Zr–O–Zr bond [40]. A broad peak around 3,500–3,000 cm^{-1} was assigned to stretching vibration of O–H groups on sample surface [20]. The peak at 1,630 cm^{-1} corresponds to the vibration of O–H bonds [41] and the one at around 1,338 cm^{-1} may be referred to non-bridging –OH groups on the surface [42]. The NH_2–ZrO_2 sample showed new peaks at about 2,928; 1,548 cm^{-1} and at 1,025 cm^{-1}. The peak at 2,928 cm^{-1} corresponds to C–H stretching vibration [43]. The peak at 1,630 cm^{-1} of ZrO_2 shifted to 1,548 cm^{-1} after functionalization which can be associated with the bending mode of N–H bond [44] and another low-intensity peak also appeared on the shoulder of ZrO_2 peak at around 1,118 cm^{-1} which is assigned to the C–N bond [45] while the peak appearing at 1,025 cm^{-1} corresponded to Si–O–Zr bond [41]. The FTIR spectra after adsorption of Cr(VI) showed two new peaks at 1,627 and 938 cm^{-1}. The peak at 1,627 cm^{-1} is attributed to the stretching vibration of Cr=O [46], while the peak at 938 cm^{-1} indicates the resonance of Cr–O and Cr=O which confirms the presence of $HCrO_4^-$ [47].

3.1.4. TGA/DTA analysis

The TGA/DTA thermograms of nanocrystalline ZrO_2 and NH_2–ZrO_2 are presented in Figs. 5a and b, respectively. The TGA of ZrO_2 shows the weight loss in two steps. The first weight loss occurs in the temperature range of 30°C–86°C while the second weight loss is observed in the range of 170°C–250°C. The weight loss in both regions is attributed to the desorption of adsorbed water from the sample surface and pores [48]. The appearance of two endothermic peaks in the DTA thermogram confirmed that both the weight loss is endothermic. No obvious weight loss is observed from 250°C to 700°C, which reflects the high thermal stability of nano-crystalline ZrO_2. Furthermore, the TGA

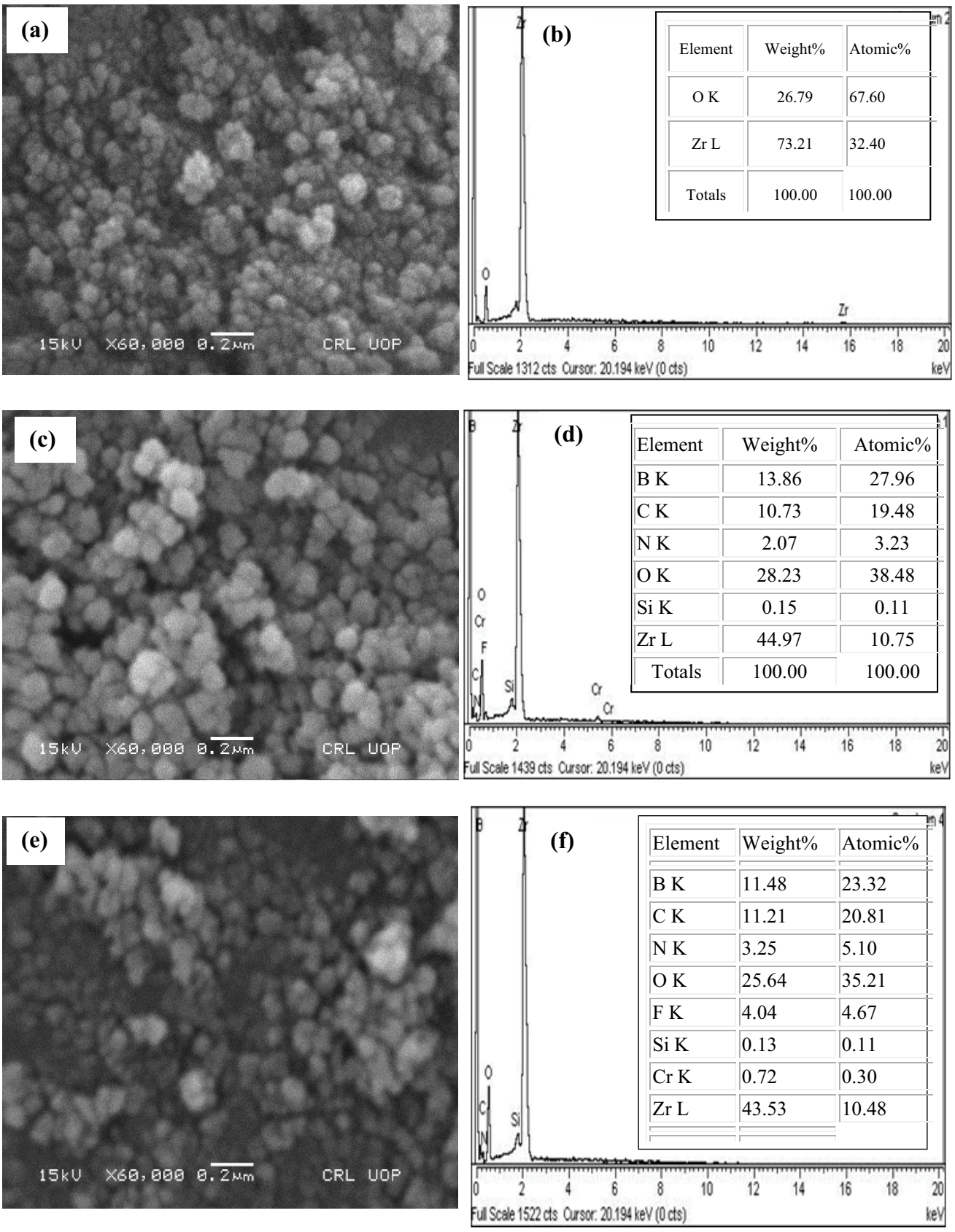

Fig. 3. SEM image (a) and EDX spectrum (b) of ZrO_2, SEM image (c) and EDX spectrum (d) of NH_2–ZrO_2 before adsorption, SEM image (e) and EDX spectrum of Cr(VI) loaded NH_2–ZrO_2 (f).

thermograms of NH_2–ZrO_2 show two major weight losses in the temperature range of 30°C–70°C and 250°C–470°C. The first weight loss is attributed to the physically adsorbed water on the surface of NH_2–ZrO_2 while the second weight loss is assigned to the decomposition of amines groups on the surface of zirconia. The DTA curve shows two peaks which confirm the endothermic nature of both the weight losses. Similar TGA analysis was reported by Liu et al. [49] for amino functionalized zirconia.

3.1.5. Point of zero charge (pH_{PZC})

Salt addition method [28] was used to find out the pH_{PZC} of NH_2–ZrO_2. The change in pH values were plotted vs. pH_i values. The pH_{pzc} of NH_2–ZrO_2 is 9.3, which is comparable to that of amino functionalized titanate nanotubes reported by Niu et al. [50].

3.2. Adsorption studies

The effect of different process parameter such as solution pH, temperature, adsorbent dose, contact time, and electrolyte concentration on adsorption of Cr(VI) on NH_2–ZrO_2 is presented in Figs. 6a–e.

3.2.1. Effect of solution pH

The effect of solution pH on adsorption of Cr(VI) onto NH_2–ZrO_2 was examined within the pH range 2–11 at 298 ± 1 K and the results obtained are shown in Fig. 6a. The percent removal of Cr(VI) was affected significantly by solution pH and maximum removal was seen in the most acidic condition. The percent removal of Cr(VI) decreased from 92.49% to 17.23% when the pH was changed from 2 to 11 ± 0.1. The higher removal efficiency at lower pH is attributed to the electrostatic interactions between oppositely charged chromate ions and adsorbent surface. The decrease in percent removal at higher pH is associated with the pH_{pzc} of adsorbent. The pH_{pzc} of NH_2–ZrO_2 is 9.3 which indicate that at lower pH, the surface is highly protonated. As the pH value increases, the surface protonation weakens leading to a decrease in adsorption capacity of adsorbent. Sun et al. [51] also reported similar effect of pH on chromate adsorption onto amino functionalized magnetic cellulose nanocomposite.

3.2.2. Effect of Cr(VI) initial concentration and temperature

The effect of initial concentration on adsorption of Cr(VI) by NH_2–ZrO_2 was studied in the range 9.90–283.20 mg/L at three different temperatures at pH 2 ± 0.1. The experimental results (Fig. 6b) shown that the adsorption capacity of NH_2–ZrO_2 for Cr(VI) uptake increases initially with increase in chromate ions concentration and then the curve shows a bent beeline, indicating that no further adsorption take place. The primary increase in chromate ion adsorption is accredited to the high driving force, which overcome all the mass transfer resistance of chromate ions between aqueous phase and available surface-active sites. The bent beeline in the curve showed that the surface of adsorbent is saturated with chromate ions and there are no

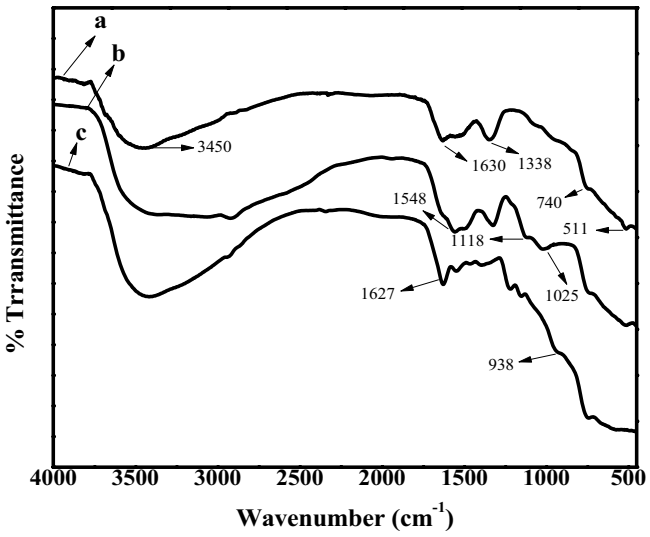

Fig. 4. FTIR spectra of (a) ZrO_2, (b) NH_2–ZrO_2, and (c) Cr(VI) loaded NH_2–ZrO_2.

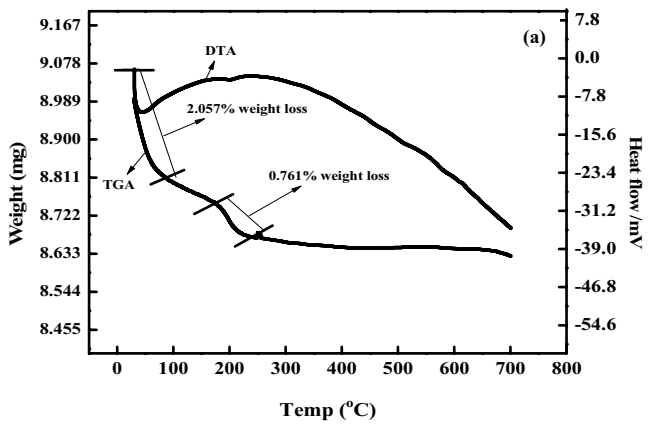

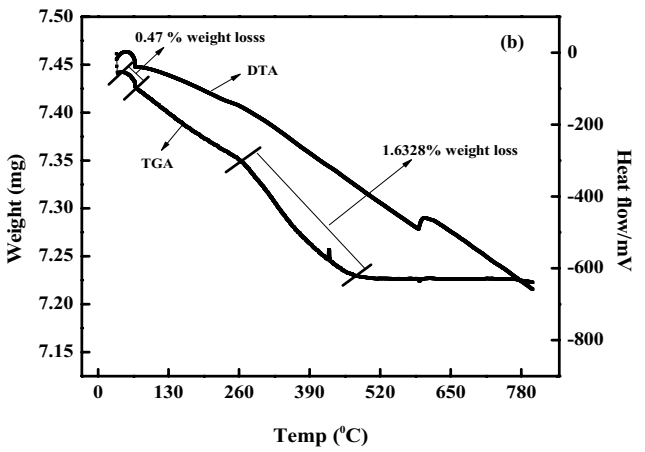

Fig. 5. TGA/DTA curves of (a) ZrO_2 and (b) NH_2–ZrO_2.

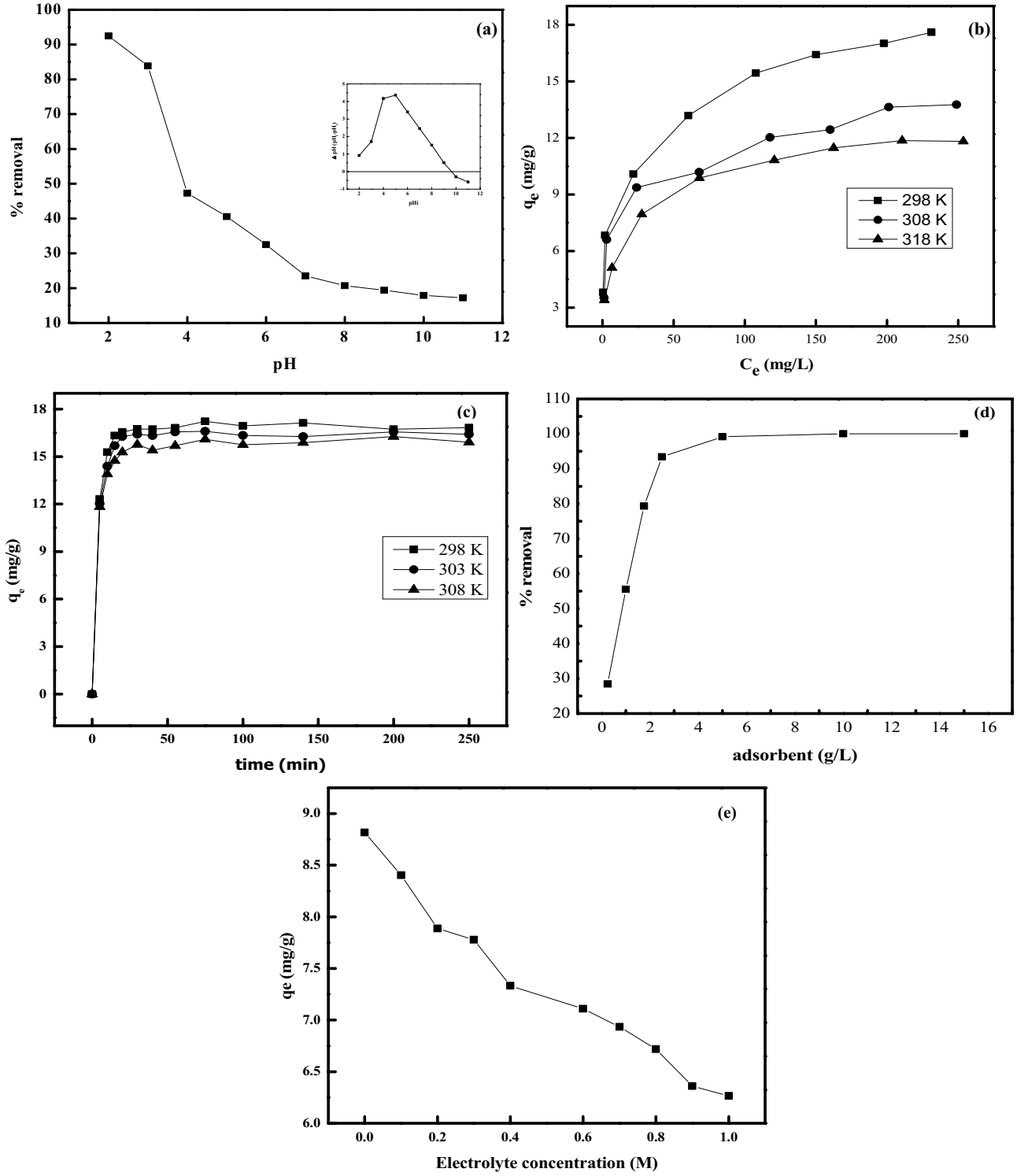

Fig. 6. Effect of (a) solution pH, (b) Cr(VI) initial concentration and temperature, (c) contact time, (d) adsorbent dose, and (e) electrolyte concentration on adsorption of Cr(VI) by NH_2–ZrO_2.

more adsorptive sites available. Lou et al. [52] have reported similar results using amino functionalized halloysites for Cr(VI) adsorption.

To investigate the effect of temperature on adsorption of Cr(VI) by NH_2–ZrO_2, the adsorption experiments were conducted at 298, 308, and 318 ± 1 K (Fig. 6b). It can be observed that Cr(VI) adsorption decreases with rise in temperature. The decrease in adsorption with rising in temperature, confirmed exothermic behavior of Cr(VI) adsorption by NH_2–ZrO_2. At high temperature, the interaction

between chromate ions and NH_2–ZrO_2 weakens, and the solubility of adsorbed species increases, leading to the decrease in adsorption capacity. Wang et al. [53] also reported similar findings for Cr(VI) adsorption using amino functionalized titanate nanotubes.

3.2.3. Effect of contact time

The effect of contact time on Cr(VI) adsorption by NH_2–ZrO_2 was investigated at different temperatures (298, 303, and 308 K) at pH 2 ± 0.1 and Cr(VI) initial concentration of 197 mg/L as shown in Fig. 6c. It can be seen that the uptake capacity of Cr(VI) is highly dependent on contact time and was found to increase significantly with time. The uptake was rapid in initial time intervals and then decreased steadily until equilibrium point is achieved. The equilibrium was reached in about 50 min. The high adsorption rate at initial intervals can be related to the presence of excess binding sites on NH_2–ZrO_2 surface. These sites then rapidly decrease with time which results in slow adsorption rate and finally attained a constant value. The slow adsorption rate near the equilibrium point may be due to electrostatic repulsion between different hexavalent species of chromium such as $HCrO_4^-$, CrO_4^{2-}, $HCr_2O_7^-$, and $Cr_2O_7^{2-}$ already adsorbed on NH_2–ZrO_2 surface and in the solution [2].

3.2.4. Effect of media dosage and electrolyte concentration

Effect of media dose on the removal efficiency of Cr(VI) by NH_2–ZrO_2 was examined at initial chromate ion concentration of 24.545 mg/L at pH 2 ± 0.1 as shown in Fig. 6d. The amount of adsorbent added to the solutions was in the range of 0.25–15 g/L. The plot shows a direct relationship between percentage removal of Cr(VI) and adsorbent dose. The % removal increased to 93.45% and 99.17% at media dose of 2.5 and 5 g/L, respectively. The enhancement in % removal with increase in media dose is ascribed to the availability of more adsorptive sites.

Wastewater contains several types of ions in significant amounts which can affect the adsorption of Cr(VI). The effect of $NaNO_3$ on adsorption of Cr(VI) was investigated at pH 2 ± 0.1. The results (Fig. 6e) indicate that the uptake of Cr(VI) on NH_2–ZrO_2 decreases significantly with rising $NaNO_3$ concentration. The decrease in adsorption efficiency is attributed to the competition between chromate and electrolyte anions for the surface-active sites of adsorbent [49]. The study also supports that Cr(VI) adsorbed on adsorbent surface is in anionic form.

3.2.5. Mechanism of adsorption

Hexavalent species of chromium exists in various forms depending upon the concentration and pH of solution. Different forms of Cr(VI) are H_2CrO_4, $HCrO_4^-$, CrO_4^{2-}, $HCr_2O_7^-$, and $Cr_2O_7^{2-}$ which are a function of solution pH. The equilibrium among these species is expressed [54] as:

$$H_2CrO_4 \rightleftharpoons HCrO_4^- + H^+ \qquad K_1 = 1.58 \times 10^{-1} \qquad \text{(i)}$$

$$HCrO_4^- \rightleftharpoons CrO_4^{2-} + H^+ \qquad K_2 = 3.16 \times 10^{-7} \qquad \text{(ii)}$$

$$2HCrO_4^- \rightleftharpoons Cr_2O_7^{2-} + H_2O \qquad K_3 = 3.31 \times 10 \qquad \text{(iii)}$$

$$HCr_2O_7^- \rightleftharpoons Cr_2O_7^{2-} + H^+ \qquad K_4 = 1.17 \qquad \text{(iv)}$$

A close look of above equations shows that Eq. (iii) is independent of solution pH and depends on Cr(VI) concentration. Furthermore, H_2CrO_4 will be dominant species when solution pH values are less than 1, $HCrO_4^-$ will be dominant species when pH values are in the range of 1–6, while CrO_4^{2-} will be dominant species when solution pH values are above 6. The following tentative mechanism was proposed for the adsorption of chromate ions on NH_2–ZrO_2.

$$ZrO_2\text{–}NH_3^+ + HCrO_4^- \rightleftharpoons ZrO_2\text{–}NH_3^+ \ldots\ldots HCrO_4^- \qquad \text{(v)}$$

$$ZrO_2\text{–}NH_3^+ + CrO_4^{2-} \rightleftharpoons [ZrO_2\text{–}NH_3^+ \ldots\ldots CrO_4^{2-}]^{1-} \qquad \text{(vi)}$$

$$ZrO_2\text{–}NH_3^+ + Cr_2O_7^{2-} \rightleftharpoons [ZrO_2\text{–}NH_3^+ \ldots\ldots Cr_2O_7^{2-}]^{1-} \qquad \text{(vii)}$$

However, Eq. (v) represents the most probable mechanism of Cr(VI) adsorption onto NH_2–ZrO_2 in the present study as Cr(VI) adsorption was carried out at pH 2, at which $HCrO_4^-$ is the ruling molecular anion. Similar mechanism was proposed by Sun et al. [51] while studying the adsorption of Cr(VI) on amino-functionalized magnetic cellulose nanocomposite.

3.2.6. Adsorption kinetics studies

To study the kinetics of Cr(VI) adsorption onto NH_2–ZrO_2 different kinetic models such as pseudo-first-order, pseudo-second-order, and Elovich kinetic model were used and the plots obtained are given in Figs. 7a–c. The uptake capacity (q_e), rate constant K_1, K_2, and Elovich model parameter, A, B, and the R^2 values obtained from the above plots are summarized in Table 1. The pseudo-first-order and Elovich kinetic models do not fit well the sorption data with the theoretical and actual q_e values were not in close agreement and have lower correlation coefficients (R^2) values (Table 1) which confirms that the current data does not follow these models.

Pseudo-second-order kinetic model was also used to test the kinetics data. The plot of t/q_t vs. t shows linear relationship with high regression constant values ($R^2 > 0.999$), shows good quality of linearization. The values of q_e and K_2 were calculated from slope and intercept of the linear plot t/q_t vs. t, (Fig. 7b) and the values obtained are listed in Table 1. As can be seen, the close agreement between the theoretical and experimental q_e values further revealed that the current adsorption kinetics results can be described very well by pseudo-second-order kinetic model. The pseudo-second-order rate constant (K_2) value decreases with increasing temperature from 298, 303, and 308 K (Table 1). The decrease in K_2 and q_e values with temperature shows exothermic nature of Cr(VI) adsorption on NH_2–ZrO_2. Sharma et al. [55] have been observed comparable behavior while studying the adsorption of Cr(VI) on Nano Al_2O_3 powder.

To better understand the mechanism of Cr(VI) adsorption onto NH_2–ZrO_2, Weber–Morris intra-particle diffusion and Boyd's models were applied for analyzing the sorption kinetic data and to confirm whether, Cr(VI) sorption is controlled by particle diffusion or film diffusion. The values of R_{id} and C_i are obtained from the slope and intercept

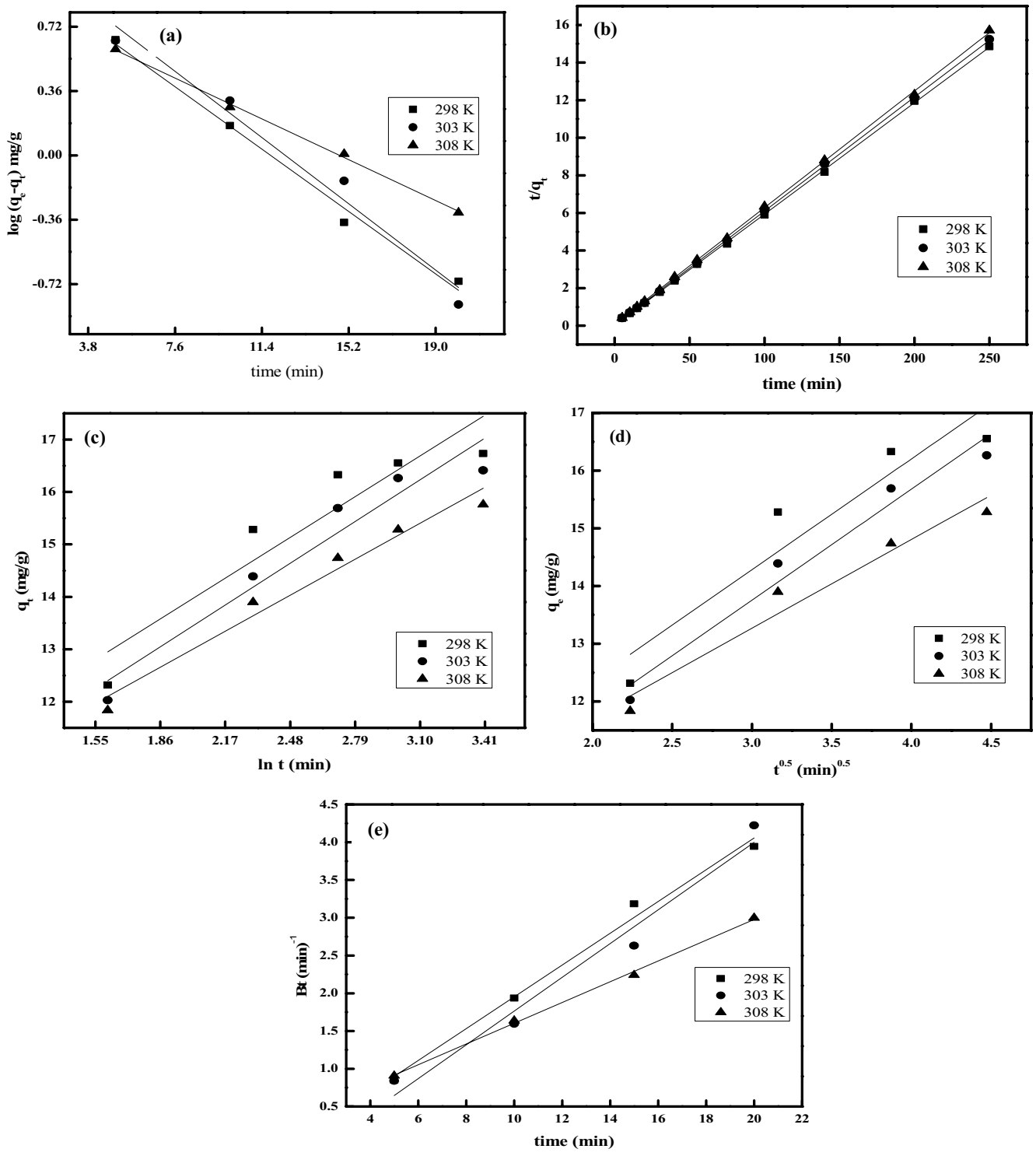

Fig. 7. (a) Pseudo-first-order, (b) pseudo-second-order, (c) Elovich, (d) intra-particle diffusion, and (e) Boyd's model plots for the adsorption of Cr(VI) on NH_2–ZrO_2.

of the plot between q_t vs. $t^{0.5}$ (Fig. 7d). As can be seen, the correlation coefficient values (Table 1) are low, and the intercept does not pass through the origin which shows, intra-particle particle diffusion is not the only rate limiting step. Sharma et al. [55] observed similar trend while studying the adsorption of hexavalent chromium on nano Al_2O_3 powder. Boyd model applied to the sorption kinetic data to further investigate the real rate-limiting step (intra-particle diffusion or film diffusion). The plot between B_t vs. t (Fig. 7e), gives a linear relationship with high correlation

Table 1
Pseudo-first, pseudo-second-order, Elovich, and intra-particle diffusion model parameters for Cr(VI) adsorption by NH_2–ZrO_2

Model	Parameters	Temperature (K)		
		298	303	308
Pseudo-first-order	Theoretical q_m (mg/g)	12.09	16.29	7.740
	Experimental q_e (mg/g)	16.75	16.41	15.76
	K_1 (min^{-1})	0.212	0.225	0.138
	R^2	0.991	0.973	0.998
Pseudo-second-order	Theoretical q_m (mg/g)	16.89	16.50	16.13
	Experimental q_e (mg/g)	16.75	16.41	15.76
	K_2 (g/min/mg)	0.171	0.087	0.046
	R^2	0.999	0.999	0.999
Elovich	q_t (mg/g) (Experimental)	16.75	16.50	16.13
	A (mg/g/min)	8.912	8.262	8.535
	B (g/mg)	2.509	2.572	2.213
	R^2	0.877	0.936	0.969
Intra-particle diffusion	K_{id} ($mg/g/min^{0.5}$)	1.919	1.924	1.538
	C_i (mg/g)	8.525	7.982	8.654
	R^2	0.900	0.968	0.958
Boyd	Rate constant (B) min^{-1}	0.210	0.223	0.137
	R^2	99.10	97.20	99.80

coefficient values. The intercepts do not pass from the origin which confirms that film diffusion is the rate-limiting step for the adsorption of Cr(VI) on NH_2–ZrO_2.

3.2.7. Adsorption equilibrium study

Different isotherm models such as Langmuir, Freundlich, Temkin, and D–R were used to study the equilibrium data and investigate mechanism of Cr(VI) adsorption onto NH_2–ZrO_2.

Langmuir isotherm model for Cr(VI) adsorption onto NH_2–ZrO_2 are shown in Fig. 8a. The plots of C_e/q_e vs. C_e were linear with high correlation coefficient values >0.999. The values of Langmuir model constants, K_b and q_m were obtained from the intercepts and slopes of the plots and are listed in Table 2. The theoretical and experimental q_m values obtained from Langmuir plot and equilibrium study are comparable which revealing that the current data fitted well to Langmuir model. It can be observed that the maximum monolayer layer adsorption capacity (q_m) and K_b values decrease with increasing temperature from 298 to 318 ± 1 K, shows exothermic nature of Cr(VI) adsorption onto NH_2–ZrO_2. Erduran et al. [56] observed similar effects for adsorption of Cr(VI) on nano-alumina powder.

The feasibility of Cr(VI) adsorption onto NH_2–ZrO_2 was tested by dimensionless separation constant (R_L) which can be expressed [54] as:

$$R_L = \frac{1}{1 + K_b C_i} \tag{22}$$

where C_i (mg/L) and K_b (L/mg) are the initial concentration of solution and Langmuir binding energy constant, respectively. The R_L value decides whether the process is favorable or not. If $R_L > 1$ the process will unfavorable, $R_L < 1$ the process will favorable and $R_L = 1$ the process is linear. In the preset study, the calculated R_L values at all temperatures were in the range of 0–1, which confirmed the favorability of Cr(VI) adsorption onto NH_2–ZrO_2.

The Freundlich isotherm model plots were linear but with lower correlation coefficient values ($R^2 > 0.97$) showing that this model does not fit well the experimental equilibrium data. The values of K_f and $1/n$ were obtained from the intercepts and slopes of the linear plots of $\log q_e$ vs. $\log C_e$ (Fig. 8b) and are summarized in Table 2. It can be observed that K_f values decreases with rise in temperature (298–318 ± 1 K) confirmed the exothermic nature of Cr(VI) adsorption on NH_2–ZrO_2. The feasibility of adsorption process was evaluated from $1/n$ values. The $1/n$ values less than 1 indicate feasible adsorption. The values of $1/n$ were less than 1 (Table 2) confirmed favorable adsorption of Cr(VI) on NH_2–ZrO_2.

The Temkin isotherm model plots Cr(VI) adsorption onto NH_2–ZrO_2 are liner with correlation coefficient values >0.97. The values of B_T and A_T were calculated from the slopes and intercepts of q_e vs. $\ln C_e$ plots (Fig. 8c). The B_T values decrease from 2.142 to 1.753 with raise in temperature from 298 to 318 ± 1 K (Table 2) due to adsorbate–adsorbent interactions which show that adsorption of Cr(VI) on NH_2–ZrO_2 is more favorable at a lower temperature.

D–R model was used to know the mechanism of Cr(VI) adsorption by NH_2–ZrO_2. D–R model assumes the adsorption heterogeneity of adsorbent surface, which makes it more general from the Langmuir model. The plot between $\ln q_e$ vs. ε^2 (Fig. 8d) showed a linear relationship with correlation coefficient values <0.90. The D–R model constants β and $q_{D–R}$ were determined from the slopes and intercepts of D–R plots. The magnitude of E gives information about

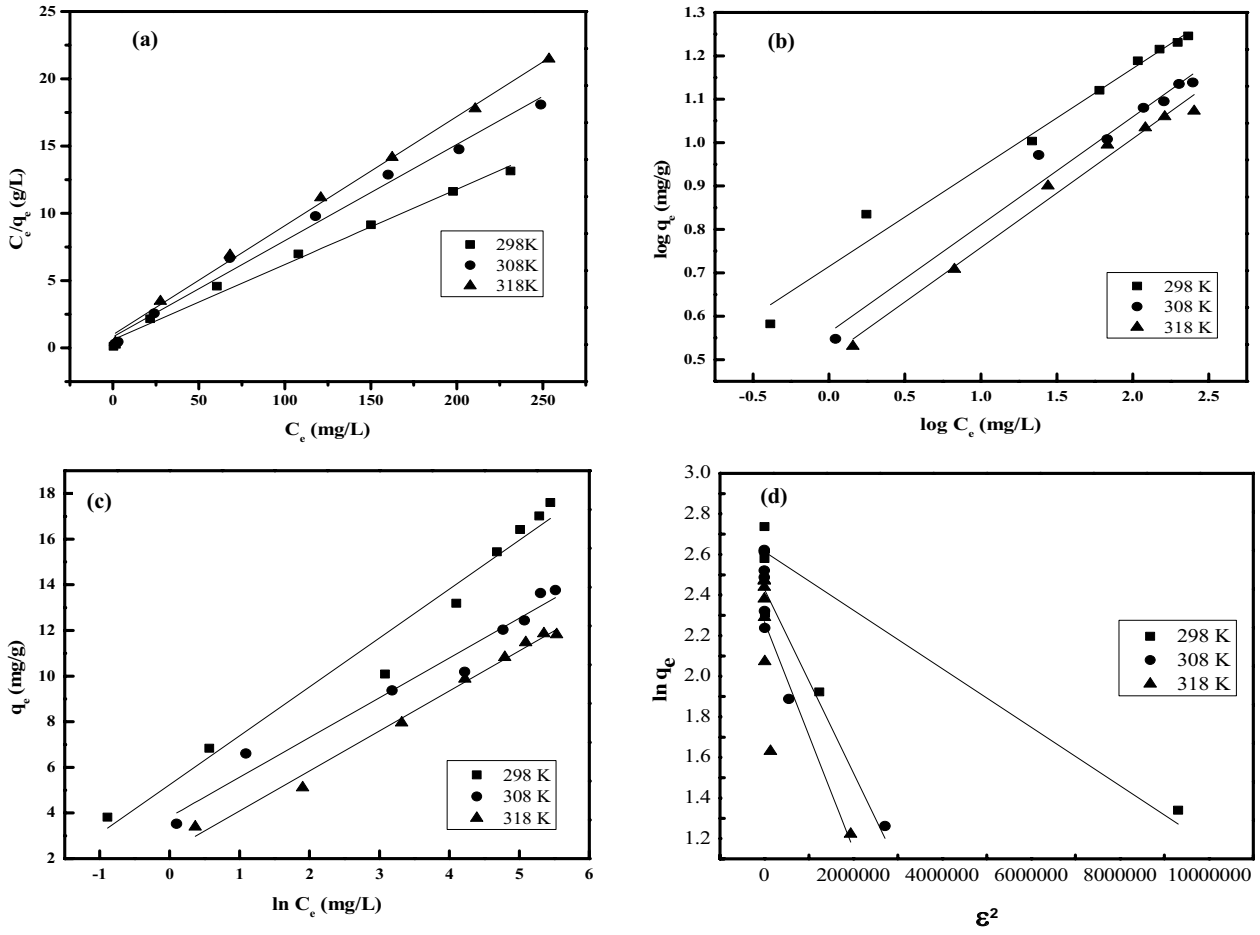

Fig. 8. (a) Langmuir, (b) Freundlich, (c) Temkin, and (d) D–R isotherm models plots for Cr(VI) adsorption onto NH_2–ZrO_2.

Table 2
Equilibrium isotherm models parameters for Cr(VI) adsorption by NH_2–ZrO_2

Model	Parameters	Temperature (K)		
		298	308	318
Langmuir	Theoretical q_m (mg/g)	17.89	13.98	12.35
	Experimental q_e (mg/g)	17.60	13.76	11.82
	K_b (L/mg)	0.092	0.087	0.082
	R^2	0.993	0.991	0.997
Freundlich	$1/n$	0.228	0.248	0.251
	n	4.385	4.023	3.986
	K_f (L/mg)	5.181	3.649	3.216
	R^2	0.993	0.977	0.986
Temkin	B_T	2.143	1.742	1.753
	b (J/mg)	1,156	1,470	1,508
	A_T (L/mg)	11.53	8.989	3.798
	R^2	0.972	0.972	0.990
D–R	q_{D-R} (mg/g)	13.65	11.35	9.67
	β (10^{-7}) (mol^2/J^2)	1.44	4.52	5.60
	E (kJ/mol)	2.24	1.00	0.91
	R^2	0.71	0.83	0.63

the mechanism and type of adsorption reaction. The value of E in the range of 8–16 kJ/mol implies ion exchange mechanism; E < 8 kJ/mol implies physio-sorption while E > 16 kJ/mol shows chemisorption. In the present case, the E values are in the range of 2.24 to 0.91 kJ/mol (Table 2) which reveals that the adsorption of Cr(VI) on NH_2–ZrO_2 is physical in nature.

3.2.8. Thermodynamic studies

The feasibility of Cr(VI) adsorption on NH_2–ZrO_2 was investigated by different thermodynamic parameters like $\Delta H°$, $\Delta S°$, and $\Delta G°$. The values $\Delta H°$ and $\Delta S°$ were calculated from the slopes and intercepts of $\ln K_d$ vs. $1/T$ plot (Fig. 9) and the values obtained are given in Table 3. The negative value of $\Delta H°$ reveals that the adsorption of Cr(VI) onto NH_2–ZrO_2 is exothermic in nature. The positive value of $\Delta S°$ shows the increase in randomness at solid–liquid interface. The negative values of $\Delta G°$ confirmed the spontaneous nature of Cr(VI) adsorption on NH_2–ZrO_2. Moreover, the decrease in $\Delta G°$ from –20.97 to –22.10 kJ/mol with rise in temperature indicates that Cr(VI) adsorption was more feasible at lower temperatures. Similar investigations have been noticed by Radjenovic and Medunic [57] during Cr(VI) sorption on carbon black.

3.2.9. Regeneration study

Regeneration is a vital criterion for investigating the efficiency and reusability of adsorbents in wastewater treatment process. Regeneration of NH_2–ZrO_2 loaded with Cr(VI) was carried out for six consecutive cycles using NaOH as desorption medium and the results obtained are presented in Fig. 10. It can be seen that NH_2–ZrO_2 has high sorption efficiency up to the fourth cycle (81.24%) which shows that NH_2–ZrO_2 has good uptake properties and reusability in removal of Cr(VI) from aqueous systems. However, in fifth and sixth cycles the Cr(VI) removal efficiency was reduced to 76.91% and 63.69%, respectively. The decrease in adsorption efficiency in the fifth and sixth cycles may be associated to the loss of some binding positions on NH_2–ZrO_2 surface caused by basic medium. Similar findings have been reported by Li et al. [58] for Cr(VI) removal by CTAB-surface-functionalized magnetic MOF@MOF composite.

3.2.10. Comparison with other adsorbents

In the present study, the adsorption capacity of NH_2–ZrO_2 (q_m) used for Cr(VI) was compared with adsorbents already reported as listed in Table 4. As can be seen, NH_2–ZrO_2 has appropriately higher uptake capacity for Cr(VI)

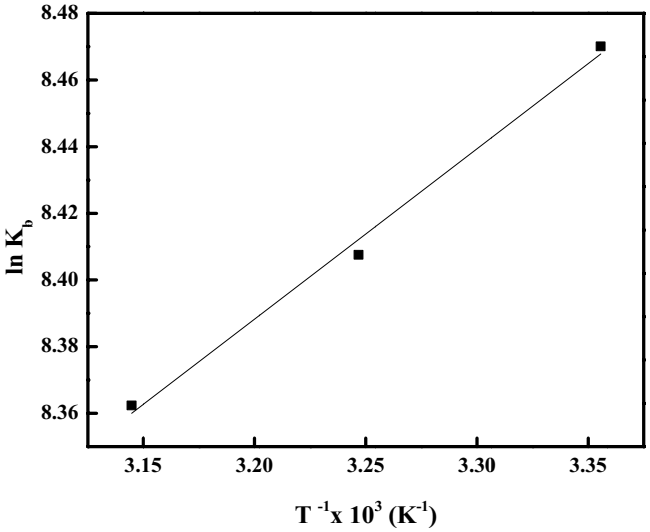

Fig. 9. Plot of lnK_b vs. T^{-1} for adsorption of Cr(VI) on NH_2–ZrO_2 at pH 2.

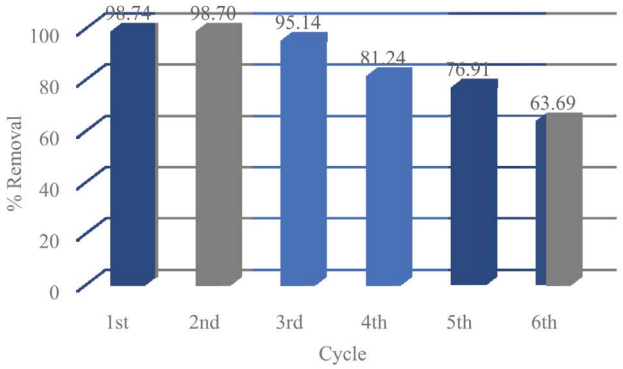

Fig. 10. Regeneration study of Cr(VI) loaded NH_2–ZrO_2 using 0.1 N NaOH solution in six consecutive cycles.

Table 3
Thermodynamic parameters for adsorption of Cr(VI) by NH_2–ZrO_2

Temperature (K)	Δ*G*° (kJ/mol)	Δ*H*° (kJ/mol)	Δ*S*° (J/mol/K)	R^2
298	–20.9786			
308	–21.9786	–4.2476	56.1444	0.994
318	–22.1069			

Table 4
Comparison of adsorption capacity of NH_2–ZrO_2 for Cr(VI) with adsorbent reported in the literature

Adsorbents	q_m (mg/g)	Reference
Starch functionalized iron oxide nanoparticles (SIONPs)	9.02	[59]
Cationic surfactant modified zeolite	12.83	[60]
SnO_2 nanoparticles	3.09	[61]
ZnO nanoparticle	9.38	[61]
Nanocrystalline ZrO_2 particles	9.68	[30]
CeO_2 micro/nanospheres	9.4	[62]
MnO_2	0.83	[63]
Mesoporous NiO nanoparticles	4.73	[64]
Amino-functionalized magnetic nano-adsorbent	11.24	[65]
Amino functionalized magnetic graphenes composite	17.29	[66]
Amino functionalized zirconia particles	17.93	Present study

than many other adsorbents described in previous studies. This shows that NH_2–ZrO_2 can be an effective adsorbent for Cr(VI) removal from wastewater.

4. Conclusions

Nano-crystalline zirconia particles was prepared by co-precipitation method and functionalized by amino groups of amino propyltriethoxy silane (APTES). The functionalized zirconia particles (NH_2–ZrO_2) can be used as an effective adsorbent for removal of Cr(VI) from aqueous solutions. The presence of carbon (10.73%), nitrogen (2.07%), silicon (0.15%), and a rise in percentage of oxygen (from 26.79% to 28.23%) in the EDX spectra of NH_2–ZrO_2 also supported by FTIR analysis, showed that ZrO_2 has been successfully functionalized with APTES. The pH_{PZC} (9.3) of NH_2–ZrO_2 revealed that it has the property of adsorption of anionic species such as chromate ions in a wide pH range. The adsorption of Cr(VI) follows the Langmuir adsorption isotherm and pseudo-second-order kinetics model. The thermodynamic parameters such as $\Delta H°$, $\Delta G°$, and $\Delta S°$ showed that Cr(VI) adsorption by NH_2–ZrO_2 is spontaneous and exothermic in nature. The values of separation factor (R_L) which were between 0 and 1 and good monolayer adsorption capacity (17.89 mg/g), confirmed that NH_2–ZrO_2 could be used as an effective adsorbent for Cr(VI) removal from wastewater as its high uptake capacity than ZrO_2 and other adsorbents reported previously. It was concluded that NH_2–ZrO_2 prepared in the present study can be used effectively for the extraction of anionic species from an aqueous environment.

Acknowledgments

The authors of this study are pleased to acknowledge the provision and support provided by the National Center of Excellence in Physical Chemistry, University of Peshawar, Pakistan for completing the research project.

References

[1] Z.A. Al-Othman, R. Ali, M. Naushad, Hexavalent chromium removal from aqueous medium by activated carbon prepared from peanut shell: adsorption kinetics, equilibrium and thermodynamic studies, Chem. Eng. J., 184 (2012) 238–247.
[2] Z.A. ALOthman, M. Naushad, R. Ali, Kinetic, equilibrium isotherm and thermodynamic studies of Cr(VI) adsorption onto low-cost adsorbent developed from peanut shell activated with phosphoric acid, Environ. Sci. Pollut. Res., 20 (2013) 3351–3365.
[3] D. Mohan, C.U. Pittman Jr., Activated carbons and low cost adsorbents for remediation of tri-and hexavalent chromium from water, J. Hazard. Mater., 137 (2006) 762–811.
[4] M.R. Abukhadra, M.A. Sayed, A.M. Rabie, S.A. Ahmed, Surface decoration of diatomite by Ni/NiO nanoparticles as hybrid composite of enhanced adsorption properties for malachite green dye and hexavalent chromium, Colloids Surf., A, 577 (2019) 583–593.
[5] S. Chatterjee, I. Sivareddy, S. De, Adsorptive removal of potentially toxic metals (cadmium, copper, nickel and zinc) by chemically treated laterite: single and multicomponent batch and column study, J. Environ. Chem. Eng., 5 (2017) 3273–3289.
[6] M. Barakat, New trends in removing heavy metals from industrial wastewater, Arabian J. Chem., 4 (2011) 361–377.
[7] R. Jayaraj, A. Suthakaran, S. Amala, C. Anbarasi, S. Selvamathan, P. Prasath, Competitive adsorption of dyes (crystal violet, methylene blue, malachite green) on chlor-alkali waste (slurry), J. Chem. Pharm. Res., 4 (2012) 1251–1258.
[8] T. Adane, D. Haile, A. Dessie, Y. Abebe, H. Dagne, Response surface methodology as a statistical tool for optimization of removal of chromium(VI) from aqueous solution by Teff (*Eragrostis teff*) husk activated carbon, Appl. Water Sci., 10 (2020) 1–13.
[9] T. Mahmood, R. Ali, A. Naeem, M. Hamayun, M. Aslam, Potential of used *Camellia sinensis* leaves as precursor for activated carbon preparation by chemical activation with H_3PO_4; optimization using response surface methodology, Process Saf. Environ. Prot., 109 (2017) 548–563.
[10] Y. He, H. Lin, M. Luo, J. Liu, Y. Dong, B. Li, Highly efficient remediation of groundwater co-contaminated with Cr(VI) and nitrate by using nano-Fe/Pd bimetal-loaded zeolite: process product and interaction mechanism, Environ. Pollut., 263 A (2020) 114479, doi: 10.1016/j.envpol.2020.114479.
[11] R. Foroutan, S.J. Peighambardoust, R. Mohammadi, M. Omidvar, G.A. Sorial, B. Ramavandi, Influence of chitosan and magnetic iron nanoparticles on chromium adsorption behavior of natural clay: adaptive neuro-fuzzy inference modeling, Int. J. Biol. Macromol., 151 (2020) 355–365.
[12] T. Zewail, S. El-Garf, Preparation of agriculture residue based adsorbents for heavy metal removal, Desal. Water Treat., 22 (2010) 363–370.
[13] Y. Su, H. Cui, Q. Li, S. Gao, J.K. Shang, Strong adsorption of phosphate by amorphous zirconium oxide nanoparticles, Water Res., 47 (2013) 5018–5026.
[14] A. Rahmani, H.Z. Mousavi, M. Fazli, Effect of nanostructure alumina on adsorption of heavy metals, Desalination, 253 (2010) 94–100.
[15] S. Debnath, U.C. Ghosh, Equilibrium modeling of single and binary adsorption of Cd(II) and Cu(II) onto agglomerated nano structured titanium(IV) oxide, Desalination, 273 (2011) 330–342.
[16] M. Fouladgar, M. Beheshti, H. Sabzyan, Single and binary adsorption of nickel and copper from aqueous solutions by γ-alumina nanoparticles: equilibrium and kinetic modeling, J. Mol. Liq., 211 (2015) 1060–1073.
[17] T. Pradeep, Noble metal nanoparticles for water purification: a critical review, Thin Solid Films, 517 (2009) 6441–6478.
[18] A.M. Hassan, W.A.W. Ibrahim, M.B. Bakar, M.M. Sanagi, Z.A. Sutirman, H.R. Nodeh, M.A. Mokhter, New effective 3-aminopropyltriethoxysilane functionalized magnetic sporopollenin-based silica coated graphene oxide adsorbent for removal of Pb(II) from aqueous environment, J. Environ. Manage., 253 (2020), doi: 10.1016/j.jenvman.2019.109658.
[19] Z.-Y. Ma, C. Yang, W. Wei, W.-H. Li, Y.-H. Sun, Surface properties and CO adsorption on zirconia polymorphs, J. Mol. Catal. A: Chem., 227 (2005) 119–124.
[20] S. Zhou, G. Garnweitner, M. Niederberger, M. Antonietti, Dispersion behavior of zirconia nanocrystals and their surface functionalization with vinyl group-containing ligands, Langmuir, 23 (2007) 9178–9187.
[21] A. Tarafdar, P. Pramanik, Synthesis of amino-functionalized mesoporous silica–zirconia mixed oxide using sodium silicate and zirconium carbonate complex, Microporous Mesoporous Mater., 91 (2006) 221–224.
[22] K. Luo, S. Zhou, L. Wu, G. Gu, Dispersion and functionalization of nonaqueous synthesized zirconia nanocrystals via attachment of silane coupling agents, Langmuir, 24 (2008) 11497–11505.
[23] J.H. Moon, Y.G. Shul, S.Y. Hong, Y.S. Choi, H.T. Kim, A study on UV-curable adhesives for optical pick-up: II. Silane coupling agent effect, Int. J. Adhes. Adhes., 25 (2005) 534–542.
[24] Z. Elbhiri, Y. Chevalier, J.-M. Chovelon, N. Jaffrezic-Renault, Grafting of phosphonate groups on the silica surface for the elaboration of ion-sensitive field-effect transistors, Talanta, 52 (2000) 495–507.
[25] M. Ostwal, R.P. Singh, S.F. Dec, M.T. Lusk, J.D. Way, 3-Aminopropyltriethoxysilane functionalized inorganic membranes for high temperature CO_2/N_2 separation, J. Membr. Sci., 369 (2011) 139–147.
[26] D. Stoltenberg, A. Seidel-Morgenstern, An attempt to alter the gas separation of mesoporous glass membranes by amine

modification, Microporous Mesoporous Mater., 154 (2012) 148–152.
[27] Y. Sakamoto, K. Nagata, K. Yogo, K. Yamada, Preparation and CO_2 separation properties of amine-modified mesoporous silica membranes, Microporous Mesoporous Mater., 101 (2007) 303–311.
[28] S. Mustafa, M. Waseem, A. Naeem, K. Shah, T. Ahmad, S.Y. Hussain, Selective sorption of cadmium by mixed oxides of iron and silicon, Chem. Eng. J., 157 (2010) 18–24.
[29] Y. Sağ, Y. Aktay, Kinetic studies on sorption of Cr(VI) and Cu(II) ions by chitin, chitosan and *Rhizopus arrhizus*, Biochem. Eng. J., 12 (2002) 143–153.
[30] D. Gusain, F. Bux, Y.C. Sharma, Abatement of chromium by adsorption on nanocrystalline zirconia using response surface methodology, J. Mol. Liq., 197 (2014) 131–141.
[31] R. Ali, T. Mahmood, S.U. Din, A. Naeem, M. Aslam, M. Farooq, Efficient removal of hazardous malachite green dye from aqueous solutions using H_2O_2 modified activated carbon as potential low-cost adsorbent: kinetic, equilibrium, and thermodynamic studies, Desal. Water Treat., 151 (2019) 167–182.
[32] T. Mahmood, S. Din, A. Naeem, S. Tasleem, A. Alum, S. Mustafa, Kinetics, equilibrium and thermodynamics studies of arsenate adsorption from aqueous solutions onto iron hydroxide, J. Ind. Eng. Chem., 20 (2014) 3234–3242.
[33] X. Rong, F. Qiu, J. Qin, H. Zhao, J. Yan, D. Yang, A facile hydrothermal synthesis, adsorption kinetics and isotherms to Congo Red azo-dye from aqueous solution of NiO/graphene nanosheets adsorbent, J. Ind. Eng. Chem., 26 (2015) 354–363.
[34] E.-H. Jang, S.P. Pack, I. Kim, S. Chung, A systematic study of hexavalent chromium adsorption and removal from aqueous environments using chemically functionalized amorphous and mesoporous silica nanoparticles, Sci. Rep., 10 (2020) 1–20.
[35] J. Gao, Q. Zhang, K. Su, R. Chen, Y. Peng, Biosorption of Acid Yellow 17 from aqueous solution by non-living aerobic granular sludge, J. Hazard. Mater., 174 (2010) 215–225.
[36] X. Chen, Modeling of experimental adsorption isotherm data, Information, 6 (2015) 14–22.
[37] M. Sadiq, M. Ali, R. Aman, H.U. Rashid, M.N. Umar, Kinetic Study of selective gas-phase oxidation of isopropanol to acetone using monoclinic ZrO_2 as a catalyst, Quím. Nova, 38 (2015) 891–895.
[38] E. Guerrini, S. Vallini, A. Colombo, S.P. Trasatti, S. Trasatti, Anodic films containing zirconia nanoparticles for corrosion protection of AA1050 aluminum alloy, J. Solid State Electrochem., 18 (2014) 1457–1468.
[39] M. Stoia, P. Barvinschi, L. Barbu-Tudoran, A. Negrea, F. Barvinschi, Influence of thermal treatment on the formation of zirconia nanostructured powder by thermal decomposition of different precursors, J. Cryst. Growth, 381 (2013) 93–99.
[40] F. Heshmatpour, R.B. Aghakhanpour, Synthesis and characterization of nanocrystalline zirconia powder by simple sol–gel method with glucose and fructose as organic additives, Powder Technol., 205 (2011) 193–200.
[41] S. Kongwudthiti, P. Praserthdam, W. Tanakulrungsank, M. Inoue, The influence of Si–O–Zr bonds on the crystal-growth inhibition of zirconia prepared by the glycothermal method, J. Mater. Process. Technol., 136 (2003) 186–189.
[42] M. Taheri, L. Maleknia, N.A. Ghamsari, A. Almasian, G.C. Fard, Effect of zirconium dioxide nanoparticles as a mordant on properties of wool with thyme: dyeing, flammability and antibacterial, Orient. J. Chem., 31 (2015) 85–96.
[43] M. Irani, A.R. Keshtkar, M.A. Moosavian, Removal of cadmium from aqueous solution using mesoporous PVA/TEOS/APTES composite nanofiber prepared by sol–gel/electrospinning, Chem. Eng. J., 200 (2012) 192–201.
[44] H. Sudrajat, S. Babel, H. Sakai, S. Takizawa, Rapid enhanced photocatalytic degradation of dyes using novel N-doped ZrO_2, J. Environ. Manage., 165 (2016) 224–234.
[45] Q. Chen, N.L. Yakovlev, Adsorption and interaction of organo-silanes on TiO_2 nanoparticles, Appl. Surf. Sci., 257 (2010) 1395–1400.
[46] L. Zhang, Y. Zhang, Adsorption characteristics of hexavalent chromium on HCB/TiO_2, Appl. Surf. Sci., 316 (2014) 649–656.
[47] A.G. Khiratkar, S.S. Kumar, P.R. Bhagat, Designing a sulphonic acid functionalized benzimidazolium based poly (ionic liquid) for efficient adsorption of hexavalent chromium, RSC Adv., 6 (2016) 37757–37764.
[48] M.E. Mahmoud, A.E. Abdou, G.M. Nabil, Facile microwave-assisted fabrication of nano-zirconium silicate-functionalized-3-aminopropyltrimethoxysilane as a novel adsorbent for superior removal of divalent ions, J. Ind. Eng. Chem., 32 (2015) 365–372.
[49] G. Liu, C. Wu, X. Zhang, Y. Liu, H. Meng, J. Xu, Y. Han, X. Xu, Y. Xu, Surface functionalization of zirconium dioxide nano-adsorbents with 3-aminopropyl triethoxysilane and promoted adsorption activity for bovine serum albumin, Mater. Chem. Phys., 176 (2016) 129–135.
[50] H. Niu, Y. Cai, Preparation of amino-modified titanate nanotubes and its striking adsorption ability to duplex DNA, J. Nanopart. Res., 13 (2011) 39–43.
[51] X. Sun, L. Yang, Q. Li, J. Zhao, X. Li, X. Wang, H. Liu, Amino-functionalized magnetic cellulose nanocomposite as adsorbent for removal of Cr(VI): synthesis and adsorption studies, Chem. Eng. J., 241 (2014) 175–183.
[52] P. Luo, J.-s. Zhang, B. Zhang, J.-h. Wang, Y.-f. Zhao, J.-d. Liu, Preparation and characterization of silane coupling agent modified halloysite for Cr(VI) removal, Ind. Eng. Chem. Res., 50 (2011) 10246–10252.
[53] L. Wang, W. Liu, T. Wang, J. Ni, Highly efficient adsorption of Cr(VI) from aqueous solutions by amino-functionalized titanate nanotubes, Chem. Eng. J., 225 (2013) 153–163.
[54] H. Shen, S. Pan, Y. Zhang, X. Huang, H. Gong, A new insight on the adsorption mechanism of amino-functionalized nano-Fe_3O_4 magnetic polymers in Cu(II), Cr(VI) co-existing water system, Chem. Eng. J., 183 (2012) 180–191.
[55] Y. Sharma, V. Srivastava, A. Mukherjee, Synthesis and application of nano-Al_2O_3 powder for the reclamation of hexavalent chromium from aqueous solutions, J. Chem. Eng. Data, 55 (2010) 2390–2398.
[56] N. Erduran, M. Gökgöz, K. Ada, Adsorption of chromium(VI) metal ions from aqueous solution using hexagonal ZnO particles: equilibrium, kinetic and thermodynamic modelling studies, Can. J. Chem. Eng., 92 (2014) 496–502.
[57] A. Radjenovic, G. Medunic, Adsorptive removal of Cr(VI) from aqueous solution by carbon black, J. Chem. Technol. Metall., 50 (2015) 81–88.
[58] L. Li, Y. Xu, D. Zhong, N. Zhong, CTAB-surface-functionalized magnetic MOF@MOF composite adsorbent for Cr(VI) efficient removal from aqueous solution, Colloids Surf., A, 586 (2020), doi: 10.1016/j.colsurfa.2019.124255.
[59] P. Singh, D. Tiwary, I. Sinha, Improved removal of Cr(VI) by starch functionalized iron oxide nanoparticles, J. Environ. Chem. Eng., 2 (2014) 2252–2258.
[60] S.L. Hailu, B.U. Nair, M. Redi-Abshiro, I. Diaz, M. Tessema, Preparation and characterization of cationic surfactant modified zeolite adsorbent material for adsorption of organic and inorganic industrial pollutants, J. Environ. Chem. Eng., 5 (2017) 3319–3329.
[61] K.Y. Kumar, H. Muralidhara, Y.A. Nayaka, J. Balasubramanyam, H. Hanumanthappa, Low-cost synthesis of metal oxide nanoparticles and their application in adsorption of commercial dye and heavy metal ion in aqueous solution, Powder Technol., 246 (2013) 125–136.
[62] J. Sun, C. Wang, L. Zeng, P. Xu, X. Yang, J. Chen, X. Xing, Q. Jin, R. Yu, Controllable assembly of CeO_2 micro/nanospheres with adjustable size and their application in Cr(VI) adsorption, Mater. Res. Bull., 75 (2016) 110–114.
[63] M. Gheju, I. Balcu, G. Mosoarca, Removal of Cr(VI) from aqueous solutions by adsorption on MnO_2, J. Hazard. Mater., 310 (2016) 270–277.
[64] M.A. Behnajady, S. Bimeghdar, Synthesis of mesoporous NiO nanoparticles and their application in the adsorption of Cr(VI), Chem. Eng. J., 239 (2014) 105–113.
[65] S.-H. Huang, D.-H. Chen, Rapid removal of heavy metal cations and anions from aqueous solutions by an amino-functionalized magnetic nano-adsorbent, J. Hazard. Mater., 163 (2009) 174–179.
[66] X. Guo, B. Du, Q. Wei, J. Yang, L. Hu, L. Yan, W. Xu, Synthesis of amino functionalized magnetic graphenes composite material and its application to remove Cr(VI), Pb(II), Hg(II), Cd(II) and Ni(II) from contaminated water, J. Hazard. Mater., 278 (2014) 211–220.